Spectral and statistical analysis of plasma turbulence: beyond linear techniques

Thierry Dudok de Wit

LCPE, UMR 6115 CNRS-Université d'Orléans, 3A, av. de la Recherche Scientifique, F-45071 Orléans cedex 2, France

published in: J. Büchner, C. T. Dum and M. Scholer (eds.),
Space Plasma Simulation, Springer, Berlin (2003)

Abstract. The analysis of plasma turbulence has traditionally been based on limited set of techniques: spectral analysis, correlation analysis, etc. This text gives a short overview of what can be done with more "advanced" techniques, i.e. techniques that exploit nonlinear properties of the data.

1 Linear vs nonlinear world

Although linear descriptions traditionally constitutes a rule of conduct in the analysis of space plasma data, there is clear evidence that nonlinear descriptions may often provide considerable added value. The problem of characterizing nonlinear processes from experimental or simulation data has in the last decade received considerable attention. This field of study is often referred to as "nonlinear time series analysis" because the sequences of observations are generally time series.

Linear descriptions can all be cast within the single convenient framework of Fourier analysis, which includes quantities such as power spectra and autocorrelation functions. There is no such single framework, however, for making nonlinear descriptions. A key problem in nonlinear world therefore is the choice of the right technique, or equivalently, the right invariant. Physical guidance is a must here. For simulation data, the underlying model can sometimes provide such guidance, but we shall not make this assumption here.

The number of time series analysis techniques is huge and increases by the day, see for example [1,35,57]. Only a small subset of these techniques, however, is actually relevant for space plasma applications. By relevant we mean that:

- a clear physical interpretation can be given to the output of the technique;
- the assumptions underlying the technique are compatible with the properties of the data.

Some applications to space plasmas can be found in [24,27,22,69,70]. Most applications deal with experimental data, although they can be readily exported to simulation data. Significant advantages of the latter are generally a smaller noise level, a more flexible size of the dataset and the possibility to access quantities that cannot be properly measured experimentally. If simulation data have received comparatively less attention so far, it is not by lack of relevance, but often because we simply don't know yet how to properly handle large ensembles of multivariate data !

There exist essentially three major families of techniques, all of which have a long history in the literature on statistics or dynamical processes. They are respectively: *higher order spectra* (section 2), *higher order statistics* (section 3), and *phase-space methods*. The latter are relevant for the characterization of low-dimensional deterministic (chaotic) systems. They will not be considered, however, because this would really require another full article. Our selection is therefore somewhat arbitrary, even more so since there are many connections between all the techniques.

The domain of application of each family can be characterized by comparing the degrees of stochasticity and nonlinearity of the process of interest, see Fig. 1.

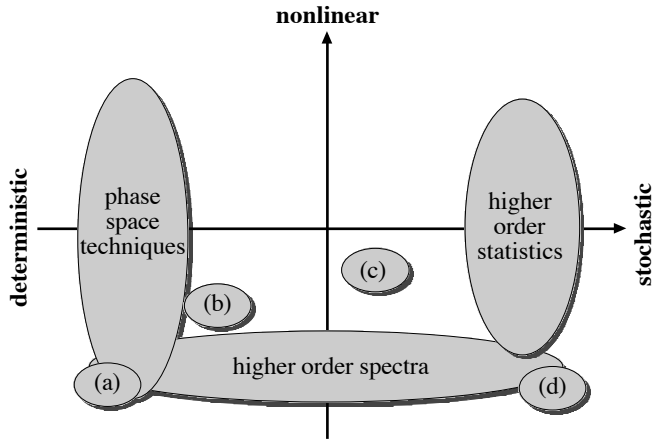

Fig. 1. Sketch of the variety of systems spanned by the properties "nonlinearity" and "stochasticity". Areas where knowledge for the analysis of time series is best available are mostly located near the borders, leaving a "no man's land" in between. Besides the two main families that are described in this text, there exist many other techniques based for example on linear oscillations (a), nonlinear Fourier transforms for solitary waves (b), hidden Markov models (c), and stochastic linear models (d). Sketch made after a figure from [57].

Note that the applicability of each technique is generally restricted to a neighbourhood around some hypothesis. The hypotheses we have chosen are the degree of nonlinearity (*how nonlinear is the process ?*) and the degree of stochasticity

(*how much is the dynamics ruled by external noise terms ?*). One could add to this the extension (*is the process temporal or spatio-temporal ?*), the number of degrees of freedom, etc.

Higher order spectra can be seen as a generalization of Fourier analysis to include information about phase coherence. This approach is particularly relevant for wave phenomena with a weak departure from nonlinearity. Typical applications are: nonlinear wave interactions, wave-particle interactions, weak turbulence, etc.

Higher order statistics although closely related to higher order spectra, are more generally applied to stochastic processes, regardless of the degree of nonlinearity. Higher order statistics are needed when the probability density departs from a Gaussian distribution. Typical applications are fully developed turbulence, fluctuations in spatio-temporal systems etc.

Phase space techniques is the name given to techniques that are generally applied to chaotic systems, i.e. to systems whose evolution in time can be modelled by a low-dimensional deterministic model. Such systems are not generic in space plasmas but the concepts that have been developed in this framework are powerful and deserve attention. Good candidates for this are particle and wavefield simulations, but successful applications to experimental data have also been reported.

2 Higher-order spectra and spectral energy transfers

One of the most obvious approaches for making the transition from a linear to a nonlinear description, consists in starting from a linear description of the system of interest, and subsequently introducing a weak nonlinearity. How far this perturbative approach can be extended to strongly nonlinear systems depends on the type of problem one is addressing.

Since one starts with a linear description, it is appropriate to describe the system in terms of its eigenmodes, namely Fourier modes. The basic assumption that underlies standard Fourier analysis is that any stationary fluctuating physical quantity can be regarded as the superposition of statistically independent Fourier modes. This means that all the relevant information is contained in the amplitude of these modes only, that is, the power spectral density (or alternatively, the autocorrelation function). If, however, there exists some parametrical or nonlinear physical process, then the phases of the Fourier modes are not independent anymore, and information is also conveyed by the phases. Higher order spectra[1] provide a means for characterizing such phase coherence [45,49,39].

2.1 Why higher order spectra ?

Let us start with an example that is based on magnetic field data as gathered by the AMPTE UKS spacecraft just upstream the Earth's quasiparallel bow

[1] higher order spectra are also called polyspectra or multispectra

shock. The dataset and its nonlinear properties are discussed in more detail in [20]. In this dataset, the turbulent wavefield is characterized by the occasional occurrence of large-amplitude structures that are preceded at their upstream edge by whistler wavetrains, see Fig. 2. This raises two questions: 1) is there a causal relationship between the whistler waves and the large structures ? 2) If such a coupling exists, are whistlers just instabilities that are triggered by the large structures or do they actually grow out of them ? Higher order spectra will answer the first question, whereas spectral energy transfers will be needed for the second.

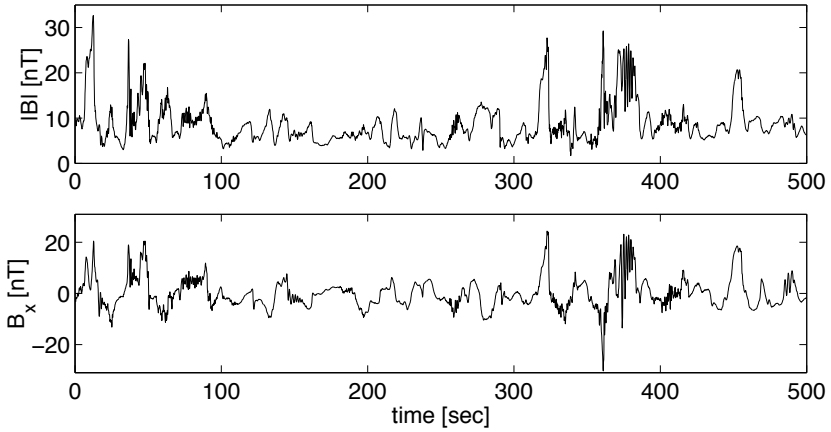

Fig. 2. Excerpt of the AMPTE magnetic field data: modulus of the magnetic field (top) and component along direction of maximum variance (bottom).

.

Higher order spectra are usually defined in the field of signal processing, using cumulants [11]. The articles by Powers and his coworkers [36,63] are good introductions, written in the framework of laboratory plasma wave experiments. Let us start with a nonlinear system, whose dynamics is a function of time t and space x, and is described by the generic model

$$\frac{\partial u(x,t)}{\partial x} = f(u(x,t)) \ , \tag{1}$$

where $f(.)$ is a continuous nonlinear and time-independent function, and $u(x,t)$ the physical quantity of interest[2]. We shall henceforth assume that $u(t)$ is stationary in time and has zero mean. By analogy with Taylor series let us decompose f into a series of linear, quadratic, cubic, and higher order functions

$$f(u) = f_1(u) + f_2(u) + f_3(u) + \cdots \tag{2}$$

[2] the spatial derivative is used here for notational convenience; one could switch time and space.

so that $f_k(\lambda u) = \lambda^k f(u)$. In a weakly nonlinear system, $f_1(u)$ should dominate over all the other terms. Wiener has shown that with mild assumptions, eq. 2 can be written as a Volterra series.

$$\begin{aligned}\frac{\partial u(x,t)}{\partial x} = &\int g(\tau_1)\, u(x,t-\tau_1)\, \mathrm{d}\tau_1 \\ &+ \iint g(\tau_1,\tau_2)\, u(x,t-\tau_1)\, u(x,t-\tau_2)\, \mathrm{d}\tau_1\, \mathrm{d}\tau_2 \\ &+ \iiint g(\tau_1,\tau_2,\tau_3)\, u(x,t-\tau_1)\, u(x,t-\tau_2)\, u(x,t-\tau_3)\, \mathrm{d}\tau_1\, \mathrm{d}\tau_2\, \mathrm{d}\tau_3 \\ &+ \cdots\end{aligned} \tag{3}$$

As we shall see later, each term can be ascribed to a different physical process. Let us now take the discrete Fourier transform in time of this series (with the notation $u_p = u(x,\omega_p)$) :

$$\frac{\partial u_p}{\partial x} = \Gamma_p u_p + \sum_{k,l} \Gamma_{kl}\, u_k u_l\, \delta_{k+l,p} + \sum_{k,l,m} \Gamma_{klm}\, u_k u_l u_m\, \delta_{k+l+m,p} + \cdots \tag{4}$$

Note how the nonlinearity couples each Fourier mode u_k to all other Fourier modes. This coupling can only occur in a specific way: for quadratic nonlinearities (the Γ_{kl} kernels), the resonance condition for interacting Fourier modes reads

$$\omega_k + \omega_l = \omega_p \ , \tag{5}$$

whereas for cubic nonlinearities we must have[3]

$$\omega_k + \omega_l + \omega_m = \omega_p \ . \tag{6}$$

A major asset of this description is the existence of analytical expressions and consequently the possibility to interpret the Volterra kernels Γ in terms of physical processes. Much work has been done in the framework of Hamiltonian systems [72] and several applications to weak plasma turbulence have been reported in [34,46]. With some additional assumptions, even the description of strong plasma turbulence can be considered, see [32].

Volterra series may in principle contain an infinite number of terms, but in many applications (and by definition in all weakly nonlinear systems) only low order terms are significant. The quadratic Volterra kernel Γ_{kl} describes *three-wave interactions* because three different Fourier modes are involved in the resonance condition (eq. 5). Two examples of such interactions are harmonic generation (the fundamental gives rise to its first harmonic) and the decay instability (a Langmuir wave decays into another Langmuir wave and an ion sound wave). In the same way, the cubic kernel Γ_{klm} describes *four-wave interactions*. The modulational instability is example of a four-wave interaction, in which a Langmuir wave decays into two other Langmuir waves plus a low-frequency ion sound wave.

[3] frequencies can be both positive and negative, so for example $\omega_k + \omega_l - \omega_p = 0$ could be rewritten as $\omega_k + \omega_l = \omega_p$

2.2 Defining higher order spectra

Volterra kernels Γ embody all the information about the nonlinear dynamics of a process, so they should be the main quantities of interest. We shall nevertheless prefer to them two other quantities. The first are *higher order spectra*, which can be obtained at low cost, using single point measurements. The second are *energy transfer functions*, which are more relevant but also more difficult to evaluate.

Let us first multiply eq. 4 by u_p^* and calculate its expectation[4]. The following series results

$$\langle \frac{\partial u_p}{\partial x} u_p^* \rangle = \Gamma_p \langle |u_p|^2 \rangle + \sum_{k+l=p} \Gamma_{kl} \langle u_k u_l u_{k+l}^* \rangle + \sum_{k+l+m=p} \Gamma_{klm} \langle u_k u_l u_m u_{k+l+m}^* \rangle + \cdots \tag{7}$$

In a homogeneous plasma the term of the left vanishes, and so we conclude that the amplitude $\langle |u_p|^2 \rangle$ is not an invariant quantity anymore but depends on all the other modes. To characterize such interactions, we must first compute the coefficients of this equation. The first term on the right is nothing but the power spectrum

$$P(\omega_p) = \langle u_p u_p^* \rangle \ . \tag{8}$$

The quadratic term gives the *bispectrum*

$$B(\omega_k, \omega_l) = \langle u_k u_l u_{k+l}^* \rangle \ , \tag{9}$$

and the cubic term is what we shall call the *trispectrum*[5]

$$T(\omega_k, \omega_l, \omega_m) = \langle u_k u_l u_m u_{k+l+m}^* \rangle \ . \tag{10}$$

Higher order spectra can therefore be seen as generalizations of the Fourier power spectrum. The bispectrum measures the amount of phase coherence between three Fourier modes that obey the frequency summation rule $\omega_k + \omega_l = \omega_p$. It vanishes if the phases of the modes are uncorrelated. Trispectra measure the amount of phase coherence between four modes.

It is often more convenient to use normalized quantities. Such a normalization can be performed in several different ways (see for example [37]). The usual approach consists in using Schwartz's inequality to define a normalized bispectrum, called *bicoherence*

$$b^2(\omega_k, \omega_l) = \frac{|\langle u_k u_l u_{k+l}^* \rangle|^2}{\langle |u_k u_l|^2 \rangle \langle |u_{k+l}|^2 \rangle} \ . \tag{11}$$

and a normalized trispectrum, called *tricoherence*

$$t^2(\omega_k, \omega_l, \omega_m) = \frac{|\langle u_k u_l u_m u_{k+l+m}^* \rangle|^2}{\langle |u_k u_l u_m|^2 \rangle \langle |u_{k+l+m}|^2 \rangle} \ . \tag{12}$$

[4] in practice the ensemble averaging can often be replaced by an averaging over time.

[5] the true definition of the trispectrum is not a fourth order moment like here, but a fourth order cumulant $T(\omega_k, \omega_l, \omega_m) = \langle u_k u_l u_m u_{k+l+m}^* \rangle - \langle u_k u_l \rangle \langle u_m u_{k+l+m}^* \rangle - \langle u_k u_m \rangle \langle u_l u_{k+l+m}^* \rangle - \langle u_k u_{k+l+m}^* \rangle \langle u_l u_m \rangle$

Both quantities are real and bounded by 0 and 1.

The interpretation of the bicoherence is the following: it measures the proportion of the signal energy at any bifrequency (ω_k, ω_l) that is quadratically phase coupled to ω_{k+l}. A large bicoherence means that the phase difference $\arg u_k + \arg u_l - \arg u_{k+l}$ reaches a fixed value, even though each phase, when taken separately, may vary in a random way. The tricoherence similarly quantifies cubic phase couplings between triplets $(\omega_k, \omega_l, \omega_m)$. Such phase couplings are a hallmark of nonlinearity, which is the main motivation for using higher order spectra.

Several applications of bicoherence to space plasmas have been reported, such as Langmuir wave coalescence in the solar wind [6], parametric instabilities in the ionosphere [60], the interaction of radio emitters with the ionosphere [40], nonlinear structures in the magnetosphere [20], simulations of beam-plasma interactions [61]. Tricoherent analysis has so far only been reported in weak turbulence simulations [37] and in magnetospheric turbulence [23].

2.3 Some properties of higher order spectra

Higher order spectra are intimately connected to higher order statistics. If a time series has a Gaussian probability density, then all higher order spectra are automatically equal to zero. Conversely, a process that has nonlinear wave interactions must necessarily give rise to a non-Gaussian probability density. The choice of the technique essentially depends on the type of coupling: if a few Fourier modes are coupled, then higher order spectra are appropriate since the deviation from Gaussianity may be weak. Conversely, if the coupling involves many different modes (e.g. in fully developed turbulence) then higher order spectra will be small whereas the probability may significantly depart from a Gaussian.

Higher order spectra have been defined so far by considering a single quantity $u(x,t)$, but they may be extended to study the phase coupling between different variables. To distinguish the two situations one should use the prefix *auto-* for a single quantity (i.e. the autobicoherence) and *cross-* for multiple quantities. Beam-plasma interactions is a typical example in which the cross-bicoherence is appropriate. According to the Zakharov equations the formation of cavitons occurs via a coupling between the electron density n and the electric field E, with $n \sim E^2$. To characterize this coupling, one must use the cross-bicoherence $B_{nE}(\omega_k, \omega_l) = \langle E_k E_l n^*_{k+l} \rangle$ and not the autobicoherence.

One of the problems encountered with higher order spectra is their representation. Because of their multivariate nature, displays in several dimensions are needed. Fortunately, one can take advantage of symmetry properties and strongly reduce the non-redundant frequency domain (called principal domain). The principal domain of the bicoherence is shown in Fig. 3 for a real signal. For the tricoherence it is a prism in 3D [48].

To illustrate these results with real data we now consider two examples:

Example 1 : We first reconsider the AMPTE magnetic field data. We know that the turbulent magnetic field contains nonlinear structures that steepen

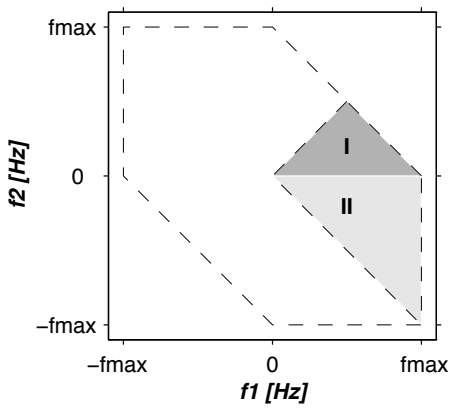

Fig. 3. Principal domain of the bicoherence. The Nyquist theorem restricts the display to the area enclosed by a dashed line. For the autobicoherence, the principal domain is I, for the cross-bicoherence it is I and II.

and progressively decay into dispersive whistler wave packets. This decay occurs via nonlinear wave interactions, and thus gives rise to phase couplings that should be detected in the wavefield autobicoherence and autotricoherence.

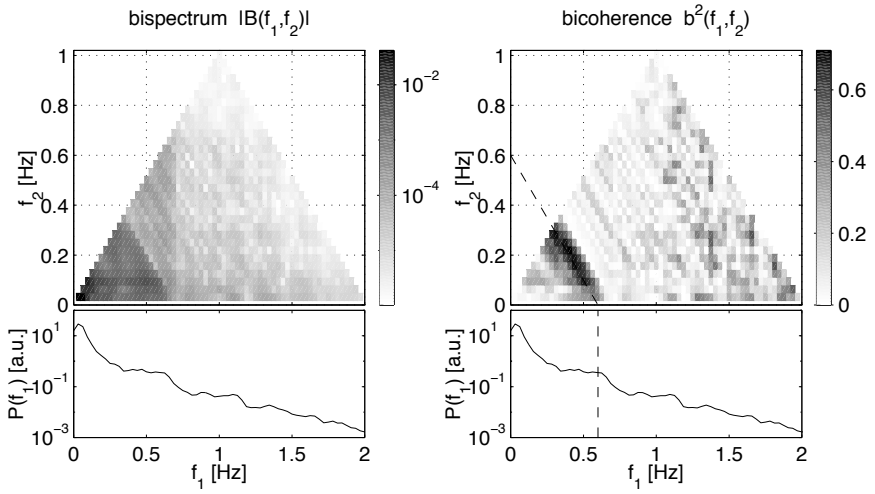

Fig. 4. Autobispectrum (left) and autobicoherence (right) of the AMPTE magnetic field data. The magnetic field component with the largest variance is analyzed and the display is restricted to the principal domain. For convenience the power spectral density is shown below each plot. The number of samples is 12000 and the display has deliberately been cut off at 2 Hz (the Nyquist frequency is 8 Hz).

Figure 4 shows the bispectrum and the bicoherence. The former reveals a featureless but significant level of wave coupling, with most of the energy concentrated in low frequency modes. The coupling strength, however, cannot be assessed by lack of normalization. The bicoherence in contrast shows a significant phase coupling between Fourier modes that satisfy the condition $f_1 + f_2 = 0.6\,\mathrm{Hz}$, with $f_1 \leq f_2 \leq 0.6\,\mathrm{Hz}$. This phase coupling implies that the large amplitude magnetic structures are somehow coupled to the whistler waves. The coupling is significant ($b^2 \approx 0.7$) but it does not reach higher levels because the nonlinear structures are embedded in a randomly fluctuating wavefield.

Example 2 : A different aspect is revealed by water level fluctuations that were recorded in a laboratory experiment. The swell results in regular and fairly monochromatic gravity waves on top of which small amplitude capillary waves are produced by wind. The bicoherence analysis of these water waves is shown in Fig. 5.

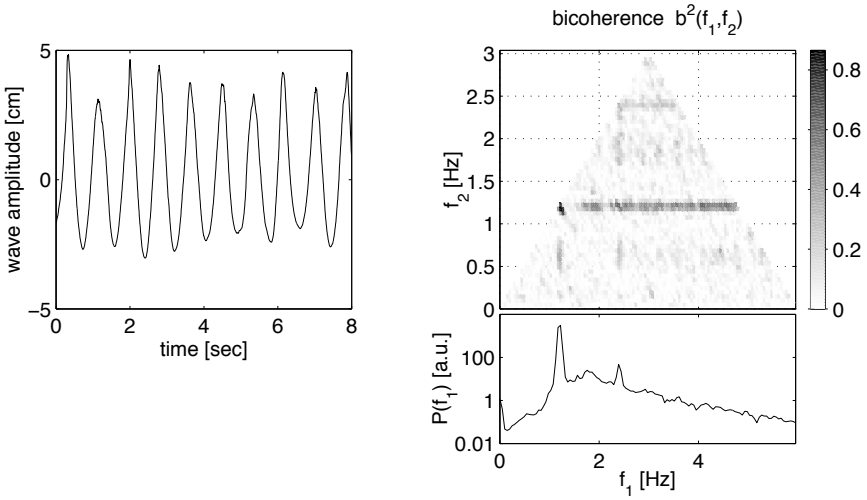

Fig. 5. Excerpt (left) and autobicoherence (right) of the water level fluctuations. For convenience the power spectral density is shown below the bicoherence. The number of samples is 65536 and the display has been cut off at 6 Hz.

The salient features of the bicoherence are a marked peak at $1.2{+}1.2 = 2.4\,\mathrm{Hz}$ and a ridge $1.2 + f = 1.2 + f$ with $f > 1.2\,\mathrm{Hz}$. The former is the classical signature of harmonic generation (the fundamental is coupled to the first harmonic). One can also distinguish peaks for higher harmonics. The ridge means that the fundamental mode is phase coupled to all modes having frequencies higher than it, and not just its harmonics. The reason for that is that the high frequency capillary waves are always located on top of the

swell (i.e. they are phase coupled to the fundamental) because this is where they are most efficiently generated by the wind.

These two examples both reveal the existence of significant phase couplings between specific Fourier modes. We must stress, however, that a phase coupling does not necessarily imply the existence of nonlinear wave interactions per se. In the first example, the ridge could be interpreted both as a decay ($0.6 \rightarrow f_1 + f_2$) or as an inverse decay ($f_1 + f_2 \rightarrow 0.6$) process. At this stage we cannot tell whether the observed phase coupling is accompanied by an energy transfer between Fourier modes (i.e. the wavefield is dynamically evolving) or whether it is just the remnant of some nonlinear effect that took place in the past or maybe even some nonlinear instrumental effect. This caveat has been highlighted by Pécseli and Trulsen [53]. Multipoint measurements are needed to unambiguously assess nonlinear wave interactions. This will be addressed shortly in section 2.6.

2.4 Estimating higher order spectra

Higher order spectra can be estimated either by direct computation of the higher order moments from Fourier transforms, or by fitting the data with a parametric model.

The **Fourier approach** is computationally straightforward: the time series is divided into M sequences, for each of which the Fourier transform is computed. An unbiased estimate of the bispectrum is then

$$\hat{B}(\omega_k, \omega_l) = \frac{1}{M} \sum_{i=1}^{M} u_k^{(i)} u_l^{(i)} u_{k+l}^{*\,(i)} \ , \tag{13}$$

The empirical estimate of the bicoherence becomes

$$\hat{b}^2(\omega_k, \omega_l) = \frac{\left| \hat{B}(\omega_k, \omega_l) \right|^2}{\sum_{i=1}^{M} \left| u_k^{(i)} u_l^{(i)} \right|^2 \sum_{i=1}^{M} \left| u_{k+l}^{(i)} \right|^2} \ . \tag{14}$$

Careful validation of higher order quantities is essential as these quantities are prone to errors. Hinich and Clay [30] have shown that the variance of the bicoherence is approximately

$$\mathsf{Var}[\hat{b}^2] \approx \frac{4\hat{b}^2}{M} \left(1 - \hat{b}^2\right) \ , \tag{15}$$

and that this quantity has a bias

$$\mathsf{bias}[\hat{b}^2] \approx \frac{4\sqrt{3}}{M} \ . \tag{16}$$

It is therefore essential to have long time series (i.e. many intervals M) in order to properly assess low bicoherence levels. This constraint becomes even more stringent for tricoherence estimates.

The need for long time series can be partly alleviated by using alternative spectral representations. Morlet wavelets, because of their better time-frequency resolution, can improve the estimates [68,20]. Nevertheless, great care should be taken in estimating higher order spectra from short or non stationary time series. It is essential that higher order spectra are averaged over many periods of the largest period of interest.

The **parametric approach** consists in fitting the time series with a parametric model, like an autoregressive (AR) model [41]. If this model correctly fits the data, the one can retrieve from it not only the spectrum but also higher order spectra. For a detailed description, see [50] and [45].

Which method is the best ? The problem of selecting the best approach is identical to that encountered in the estimation of power spectra [54]. Parametric methods are appropriate for short time series, or for time series whose spectrum and higher order spectra are either featureless (i.e. they are smooth functions of the frequency), or contain a few narrow spectral lines. Fourier methods are easier to apply and do not require any decision on the type of model that should be fitted.

2.5 Higher order spectra: more properties

Before considering spectral energy transfers and Volterra kernels, two remarks are in order. First, the bicoherence is a useful quantity for detecting asymmetries in a time series. Time-reversal asymmetries ($u(t) \leftrightarrow u(-t)$) generate imaginary bispectra only, so to detect them one should use a variant of the bicoherence

$$b_i^2(\omega_k, \omega_l) = \frac{|\Im B(\omega_k, \omega_l)|^2}{\langle |u_k u_l|^2 \rangle \langle |u_{k+l}|^2 \rangle} \ . \tag{17}$$

Up-down asymmetries ($u(t) \leftrightarrow -u(t)$) show up in the imaginary bispectrum only, so the quantity to be used is

$$b_r^2(\omega_k, \omega_l) = \frac{|\Re B(\omega_k, \omega_l)|^2}{\langle |u_k u_l|^2 \rangle \langle |u_{k+l}|^2 \rangle} \ . \tag{18}$$

The distinction between symmetries is useful for separating concurrent nonlinear processes: time-reversal asymmetries arise during nonlinear wave steepening, whereas up-down asymmetries may occur in wavefields with cavitons. These properties are illustrated in Fig. 6, which shows the "real" and "imaginary" bicoherences for the example on gravity waves. Water waves are known to have strong up-down asymmetries, and this indeed shows up in large values of the "real" bicoherence b_r^2. More surprising is the weak value of b_i^2, which indicates that the waves are still far from overturning, despite the wind strength.

A second remark concerns the generalization of higher order spectra from temporal couplings to spatio-temporal couplings. Space plasmas are truly spatio-temporal systems, so a nonlinear wave coupling should not only involve resonant frequencies, but also resonant wavenumbers. Three-wave interactions for example

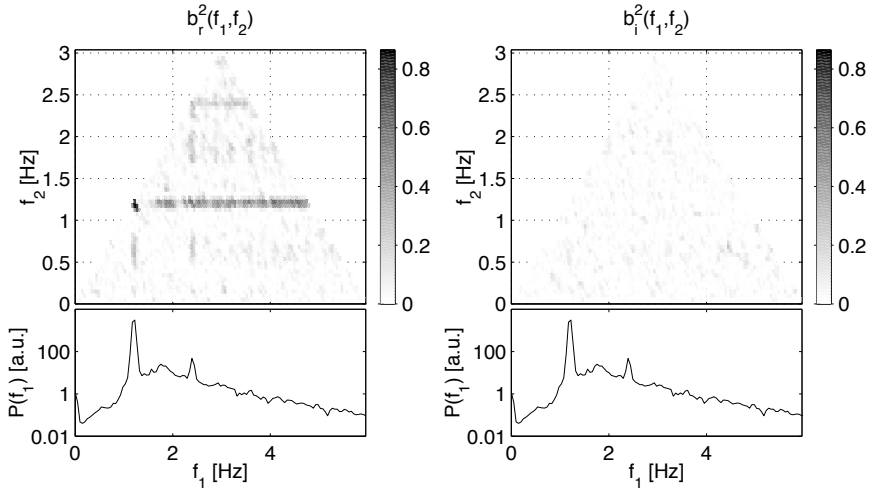

Fig. 6. Autobicoherence of the water level fluctuations (as in Fig. 5), using the real bispectrum (left) and the imaginary one (right).

can only occur between waves that satisfy four conditions

$$\begin{cases} \omega_k + \omega_l = \omega_p \\ \boldsymbol{k}_k + \boldsymbol{k}_l = \boldsymbol{k}_p \end{cases} . \tag{19}$$

The first condition can be interpreted as a conservation of energy while the second is a conservation in momentum. This resonance is illustrated in Fig. 7 for one-dimensional case. For four-wave interactions one should have

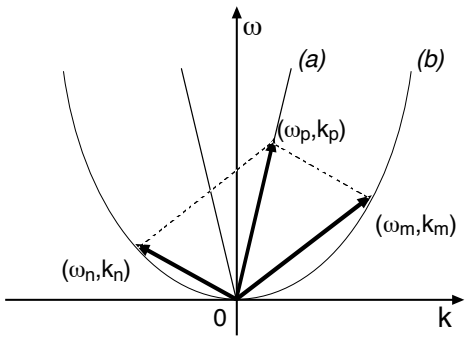

Fig. 7. Example of a plasma with two dispersion relations (a) and (b), and a possible three-wave interaction, described as vectors in (k, ω) space. Only one dimension in space is considered here.

$$\begin{cases} \omega_k + \omega_l + \omega_m = \omega_p \\ \boldsymbol{k}_k + \boldsymbol{k}_l + \boldsymbol{k}_m = \boldsymbol{k}_p \end{cases} . \tag{20}$$

Most of the time, one has access to one variable only, so that hypotheses must be made on the other. In the case of strong convection, or if the Taylor hypothesis holds, then $\omega \propto |\boldsymbol{k}|$ and so it is sufficient to consider frequencies only. If, however, the wavefield is dispersive then one cannot recover all the information from a single time series only. That is, a resonance between specific frequencies does not necessarily imply that the associated wavenumbers are also resonant.

2.6 Spectral energy transfers

One of the main shortcomings of higher order spectra is their inability to tell the origin of the phase coupling. Is it the consequence of an instrumental nonlinearity, is it the remnant of a nonlinearity that took place some time during the wavefield evolution, or does it result from an ongoing dynamical process ? To answer this question, we must go back to the Volterra kernels (eq. 3) and define a new quantity, which is called *spectral energy transfer* [64][6].

For a large ensemble of waves with different frequencies, the random phase approximation implies that

$$\langle u_p^* u_q \rangle = P_p \, \delta_{pq} \ , \tag{21}$$

where δ_{pq} is the Dirac delta function and $P_p = P(\omega_p)$ is the power spectrum. Combining this with eq. 4 gives

$$\frac{\partial P_p}{\partial x} = \gamma_p P_p + \sum_{m+n=p} T_{m,n} + \sum_{m+n+k=p} T_{m,n,k} + \cdots \tag{22}$$

This equation expresses the spatial variation in the spectral energy density at a given frequency (or wavenumber) as a sum of linear and nonlinear terms. The first term ($\gamma_p E_p$) describes linear processes, the second ($T_{m,n}$) quadratic processes, etc. The latter tells us how much energy is being transferred to ($T > 0$) or away ($T < 0$) from the p'th Fourier mode through nonlinear interactions with other modes [34].

Spectral energy transfers are probably the most relevant quantities for describing nonlinear wave interactions, but the difficulty in estimating them from experimental data has severely restricted their use so far. In contrast to higher order spectra, they require multipoint measurements and need a large and often ill-conditioned system of linear equations to be solved. Significant results have nevertheless been reported with quadratically nonlinear models in laboratory plasma turbulence [64] and for magnetospheric turbulence [23].

The numerical problems encountered in estimating spectral energy transfers can be significantly alleviated by estimating the Volterra kernels in the time domain, using parametric models, and subsequently computing the energy transfers

[6] An older article [62] provides a better introduction to the subject, but the computational scheme is outdated.

in Fourier space. The reason for that is that time-domain models are often much more efficient in capturing nonlinear features in a small number of terms.

The exists many types of nonlinear parametric models. Polynomial models offer flexibility at a reasonable computational expense. A popular class of flexible models is called Nonlinear AutoRegressive Moving Average with eXogeneous input (NARMAX) [52]. Consider two measurements that are made simultaneously and at closely spaced locations, in such a way that the time evolution of $y(t)$ is a consequence of $u(t)$. These are typically the measurements made by two spacecraft, one of which is upstream of the other: $u(t)$ is then the input signal, and $y(t)$ the output which embodies the nonlinear response of the plasma. By modelling the transfer function that relates the two signals, one can recover all the relevant nonlinear properties of the plasma, as shown by Ritz and Powers [62].

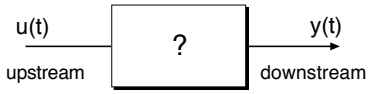

Fig. 8. The plasma behaves like a black box, which reacts to the input $u(t)$ by giving a response $y(t)$. The nonlinear properties of the plasma are recovered by modelling this response.

In practice, both $u(t)$ and $y(t)$ are continuously sampled, so a discrete transfer function model is needed. With NARMAX models the output $y_i = y(t_i)$ at a given time is expressed as a polynomial

$$y_i = \mathcal{P}[y_{i-1}, \ldots, y_{i-n}, u_i, u_{i-1}, \ldots, u_{i-n}, \varepsilon_{i-1}, \ldots, \varepsilon_{i-n}] + \varepsilon_i \ , \qquad (23)$$

where u_i is the input, ε_i the residual error between y_i and the model response, and $\mathcal{P}$ a polynomial. The output of the model thus depends on combinations involving past outputs, past and present inputs and past residual errors. A successful application of NARMAX modelling to magnetospheric turbulence (based on the AMPTE dataset of this book) was reported in [17]. The capacity of such models to fit nonlinear systems with a few (often less than a dozen) polynomial terms is clear asset. Unfortunately some of the mathematical tools associated with it are not in the public domain.

3 Higher order statistics

Higher order statistics and higher order spectra are intimately related, but they are generally used in different contexts. When a system is driven away from the linear-deterministic corner in Fig. 1, then time-domain representations are often more appropriate than spectral representations.

Most of the literature on probability theory and statistics deals with random variables whose probability density[7] function (pdf) is a Gaussian. However, Gaussian distributions is not all there is to statistics. Very often it is precisely the deviation from Gaussianity that contains pertinent information about the underlying physics. The tails of the distribution, which represent large but rare events, are of particular interest and have received much attention. Many statistical tools have been developed for this purpose. Most of them appeared in the context of turbulence [26], but new paradigms such as complexity [5], self-organization [33] and anomalous transport [10] stimulate today the development of novel tools.

3.1 Scale invariance

Symmetry is one of the key concepts behind higher order statistical analysis. Indeed, many physical systems are known to exhibit symmetries. In turbulent wavefields, for example, quantities like the velocity field often remain unchanged under the following transformation

$$\mathbf{v}(\mathbf{x}, t) \longrightarrow \lambda \mathbf{v}(\lambda^a \mathbf{x}, \lambda^b t) \tag{24}$$

Because of these symmetries, the system is said to be *scale invariant*. Roughly speaking, scale invariance means that within a wide range of (spatial or temporal) scales, it is not possible to identify a predominant scale. The property of injterest is the interplay between scales, rather than the role played by characteristic scales. This property is typical of thermodynamical systems that are at a critical point. It can be quantified in many different ways.

Spectral signatures Scale invariance can easily be expressed in the Fourier domain. Equation 24 implies that the Fourier spectra in frequency (and in wavenumber) of a scale invariant quantity behave like power laws with no characteristic cutoff frequency (or cutoff wavenumber)

$$P(\omega) \propto \omega^{-\beta} \ . \tag{25}$$

It should be stressed that this property is a necessary but not a sufficient condition. The same power law scaling should hold for all higher order spectra and structure function analysis (see below) will provide a means for getting more information.

Power laws are never observed exactly in practice. Mesoscales always provide a low-frequency cutoff (otherwise the variance of the process would diverge) whereas the high frequency cutoff is generally caused by damping or viscosity. In between, the spectrum is often corrupted by spectral lines associated with plasma waves. In spite of this, power laws extending over several decades have

[7] From a mathematical point of view, the terms *probability density* and *probability distribution* bear different meanings. Here, as in the physics literature, they are used interchangeably.

been observed in the solar wind [28]. Inside the magnetosphere, this range is generally shorter. For a power law to be meaningfully assessed in experimental data, it should be observed over at least one decade.

Equation 25 suggests that the scaling exponent or spectral index β can be directly estimated from the Fourier power spectrum. It has been shown since [3] that wavelets are better for that purpose because they are inherently self-similar. The distinction between the two approaches becomes particularly important when one has to deal with short and noise-corrupted data. Figure 9 shows an example based on a synthetic data set. A time series with $N = 512$ samples was generated with a spectral index $\beta = 2$. The figure compares the spectrum obtained by standard FFT and by using a discrete wavelet transform with Daubechies wavelets. Clearly, the latter succeeds much better in capturing the power law scaling.

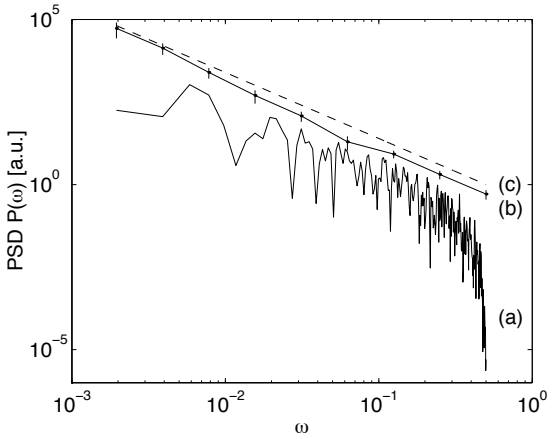

Fig. 9. Power spectral density of a synthetic time series with $N = 512$ samples and a spectral index $\beta = 2$: a) stands for standard periodogram estimate with a single Welch window, b) was obtained with 3rd order Daubechies wavelets (the scales a are converted into frequencies by $\omega = 1/a$), c) gives the exact result. The power spectra have been shifted vertically for easier comparison.

Scale-invariance and structure functions Since the spectrum is not sufficient for assessing scale invariance, it is necessary to look at higher order moments. In addition to this, one should also consider spatial gradients and higher order derivatives in order to distinguish temporal variations from spatial structures. For a stationary Gaussian process, these derivatives all must have a Gaussian pdf.

In practice, it is quite difficult to properly separate spatial structures from temporal variations, even with multipoint measurements. Therefore, instead of

computing gradients, it is customary to compute spatial increments

$$\delta \mathbf{y} = \mathbf{y}(\mathbf{x} + \mathbf{l}, t) - \mathbf{y}(\mathbf{x}, t) \ . \tag{26}$$

Furthermore, assumptions are often made to convert spatial structures into temporal dynamics. In the solar wind, for example, the turbulence is nearly frozen in the wavefield (this is better known as the Taylor hypothesis, see [26]) so that one can reasonably set $\tau = l/v$ and hence for a scalar quantity

$$\delta y = y(t + \tau) - y(t) \ . \tag{27}$$

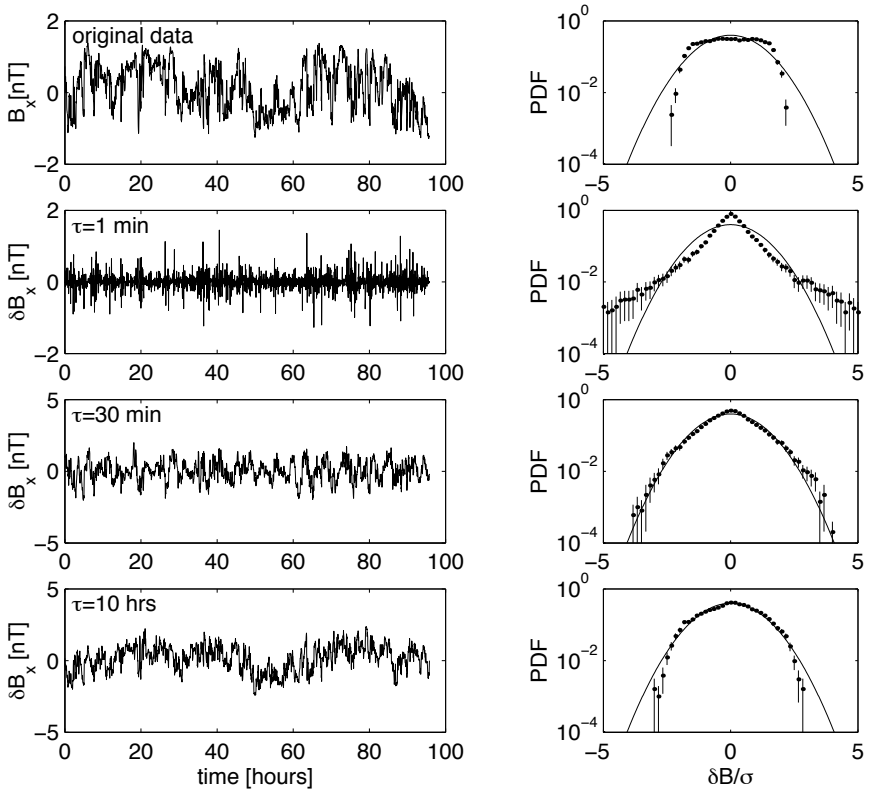

Fig. 10. Excerpt of Ulysses magnetic field data (left column) and the associated pdfs (right column). Each row corresponds to a different value of τ, the first row showing the original data. The number of samples is 20000 and the B_x component was used. different values of τ. All the pdfs have been rescaled to have unit standard deviation and zero mean; a Gaussian distribution with equal mean and standard deviation is shown for comparison. The sampling period is 1 min. and error bars correspond to ± 1 standard deviation.

Figure 10 shows an excerpt of magnetic field data gathered by Ulysses in 1994 within the solar wind from the south solar pole. The wavefield mainly consists of Alfvén waves that rotate on a sphere of constant radius, hence the peculiar pdf, which is much more akin to a uniform than to a Gaussian distribution. The pdfs of the differenced data on the contrary exhibit strongly enhanced tails. For small τ, the time series shows large bursts and the pdf is highly non-Gaussian. The larger τ is, the closer the pdfs are to the original one, because distant fluctuations are essentially independent. The study of this departure from Gaussianity is a central research issue in many fields because it is indicative of the microscopic turbulent processes.

The simplest way of quantifying the various shapes of the pdfs consists in computing their higher order moments. This is called the *structure function* approach

$$S_p(\tau) = \langle |y(t+\tau) - y(t)|^p \rangle \ . \tag{28}$$

A large amount of literature is devoted to this technique. For general references, see [51,26,9]; introductions to plasmas can be found in [8,44,14]. Structure functions can in principle be computed from any physical quantity, but a meaningful comparison against theory requires the use of natural variables. In space plasmas, the natural variables for Alfvén waves are the Elsässer variables $\mathbf{Z}^{\pm} = \mathbf{V} \pm \mathbf{V}_A$, where $\mathbf{V}_A$ is the Alfvén velocity [44].

An interesting result is the existence of a universal scaling law when the wavefield is scale-invariant

$$S_p(\tau) \propto \tau^{\alpha(p)}. \tag{29}$$

The larger order p is, the more emphasis is put on the tails of the distribution and the more difficult it becomes to measure the scaling exponent $\alpha(p)$. The range in which this scaling holds is called inertial range. Any deviation of $\alpha(p)$ from a linear dependence is an indication for irregular redistribution of the energy in the turbulent cascade. In the classical K41 model by Kolmogorov [26], the turbulent eddies are supposed to be in a state of local equilibrium: each eddy decays into smaller ones, which again give rise to smaller eddies, and so on. For this model, one obtains $\alpha = p/3$. Many theoretical models for turbulent cascades have been developed since in order to match experimental results [51,9]. The model developed by Castaing and coworkers is today widely used both in neutral fluids and in plasmas [14].

As an example, consider a turbulent cascade in which the eddies are not space filling but occupy a domain whose physical dimension is $D \leq 3$. One should then have $\alpha(p) = 3 - D + p(D-2)/3$. This property is illustrated in Fig. 11 for three cases: a) the K41 model in which each eddy is space-filling (D=3), b) the *monofractal* case in which each eddy occupies a fixed fraction of space (D is fixed), and c) the *multifractal* case in which the occupancy of space varies locally (D varies). A sparse filling of space can results from a stretching of eddies into filamentary vortices. Numerical simulations indeed support such a picture [8].

Burlaga [12] first pointed out the striking similarity between solar wind turbulence and hydrodynamic turbulence, a result confirmed since by many authors

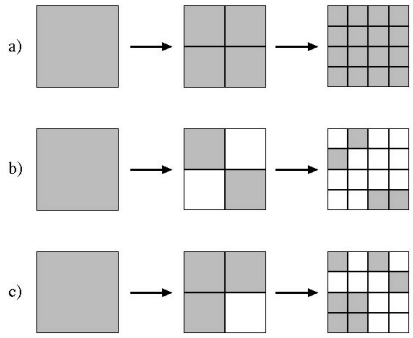

Fig. 11. Illustration of the turbulent cascade in 2D, in which each turbulent eddy (gray area) decays into four smaller eddies. Cases a) to c) respectively correspond to the the Kolmogorov K41 model with space-filling eddies, the monofractal cascade model, and the multifractal cascade model.

[43,13,31]. Structure function analysis has also been applied to other quantities, such as geomagnetic indices [67]. All these studies suggest that space plasmas are scale-invariant but that this scaling varies locally, hence the name multifractal. The macroscopic consequence of this local property is irregular behaviour with sudden bursts of activity called *intermittency*.

The structure function associated with the Ulysses data is shown in Figure 12, for orders between $p = 1$ and $p = 6$. It can be argued that an inertial range is apparent for $\tau = 3 - 30$ min. In this range, the scaling exponent is a convex function of p, which supports the multifractal character of the turbulent wavefield. The figure also shows another quantity

$$A_p(\tau) = \frac{S_p(\tau)}{S_2(\tau)^{p/2}} \ . \tag{30}$$

For a Gaussian distribution, $A_p(\tau)$ should not depend on the scale τ. This quantity confirms the existence of wide distributions for small τ and on the contrary rather narrow distributions for large τ.

Structure functions: pitfalls Structure functions suffer from a number of problems. First, theoretical models are not as easy to develop for magnetofluids as for neutral fluids. Some obstacles to a straightforward interpretation are symmetry breaking due to the magnetic field, the need to have Elsässer variables, and the questionable validity of the Taylor hypothesis in space plasmas.

Furthermore, structure functions, like all higher order quantities, become very vulnerable to outliers and lack of statistics as the order p increases. This problem has often been overlooked in the literature. It turns out that moments beyond $p = 4$ or $p = 5$ often cannot be meaningfully assessed, even with large data sets [21,31]. Therefore, great care should be taken in interpreting results.

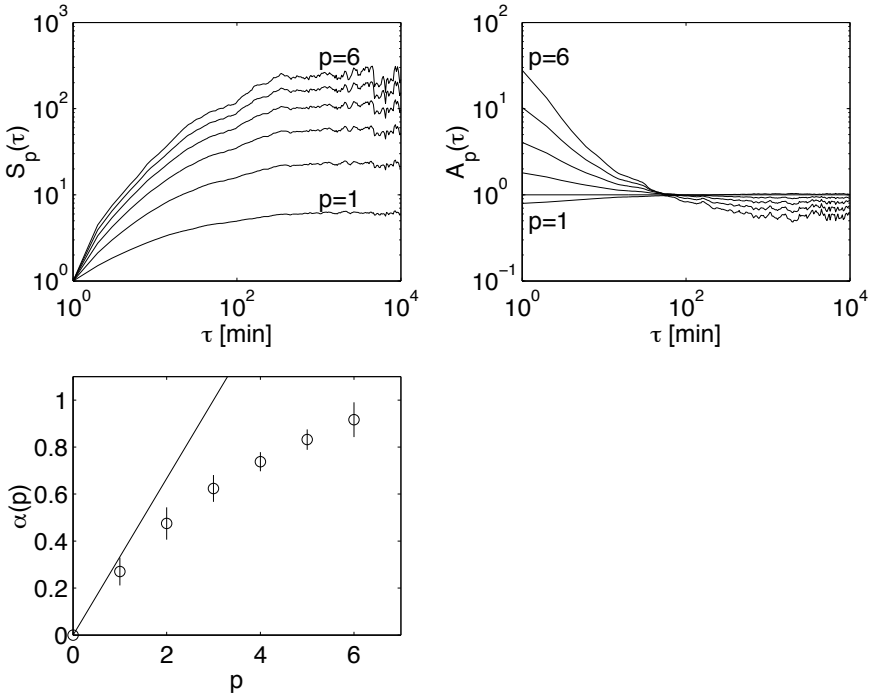

Fig. 12. Structure function analysis of Ulysses magnetic field data: the structure function $S_p(\tau)$ (top left), the normalized structure function $A_p(\tau)$ (top right), and the scaling exponent $\alpha(p)$ estimated between $\tau = 3$ and $\tau = 30$ (bottom left). The data set is the same as in Fig. 10

.

Scale invariance: beyond structure functions Structure functions have enjoyed great popularity so far, but there are many alternatives to the characterization of scale invariance. It has been shown [47] for example that structure function estimates based on wavelets perform better. The reason is to be found in the self-similar nature of wavelets.

Scale invariance can be probed by many other quantities, which are conceptually related the topology of phase space, information measures etc. Since the domain of application largely exceeds plasma physics and nonlinear time series analysis, any classification tends to be arbitrary. We just mention here multifractal analysis, whose purpose is to measure the *singularity spectrum* (or multifractal spectrum). The latter is indicative of the dimension of the region over which a spectral index β of a given value is observed. Singularity spectra are in turn connected to generalized dimensions [5]. Figure 13 shows an example of singularity spectrum that was computed by Consolini [18] from the auroral electrojet (AE) geomagnetic index. For a monofractal process, only one value of

β should occur, whereas we observe a broad distribution of values that indicative of a multifractal process.

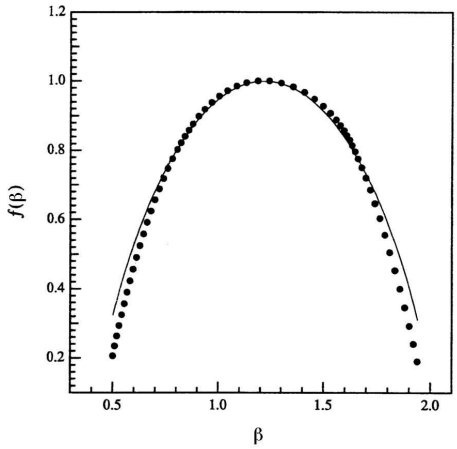

Fig. 13. Singularity spectrum from auroral electrojet data. Dots are experimental data points and the line comes from a model that is based on a two-scale Cantor set. Figure adapted from [18].

The robust estimation of singularity spectra is a delicate task and validation is not straightforward. The estimation of singularity spectra can be done in various ways, e.g. [16]. These techniques are outperformed today by a wavelet method called *wave transform modulus maxima* [4].

Finally, let us mention the theory of large deviations [66] as an alternative approach to the modelling of pdfs with long tails. Its relevance for many geophysical phenomena (such as earthquakes) may well extend to space plasmas.

3.2 Long-range dependence and self-organized criticality

Long-range dependence is just another manifestation of scale invariance. But, since it is often studied in connection with Self-Organized Criticality (SOC), it deserves a section on its own.

The SOC paradigm has recently enjoyed great popularity as a possible explanation for a wide range of phenomena that are observed in complex systems. SOC occurs in spatially-extended metastable systems, in which small perturbations can trigger fluctuations or avalanches of any size. The main signatures of SOC are scale invariance and long-range correlations, and a fractal topology (i.e. a self-similar spatial structure). For a general reference on SOC, see [33] and for a discussion on the quantification of long-range dependence see [7]. Whether SOC is really applicable to space plasma phenomena is still a matter of controversy; meanwhile, some fingerprints of SOC have been identified in magnetospheric dynamics [71,19].

Spectral signatures Processes with long-range dependence are sometimes termed $1/f$ processes because their power spectra generally exhibit a power law scaling $P(\omega) \propto \omega^{-\beta}$ with a spectral index β that is close to 1. Therefore, a necessary (but not a sufficient) condition for having long-range dependence is to observe spectra that follow a power law down to the smallest frequencies (or wavenumbers). A cutoff will always eventually appear due to the finite size of the system.

As discussed before in Sec. 3.1, the estimation of the spectral index β should be done with great care. In particular, estimators based on wavelets [3] should systematically be preferred.

Figure 14 shows an application to the AE geomagnetic index, a quantity that is often used because of its close connection with the dynamics of substorms. One year of one-minute resolution data were analyzed. The Fourier spectrum reveals a broken power law, with approximately a ω^{-2} scaling at high frequencies and a ω^{-1} scaling below. The wavelet-based spectrum gives much better evidence for this broken power law, and in addition reveals the cutoff frequencies more evidently. The spectrum eventually saturates around a period of a few tens of days, which is likely to be associated with the solar rotation period. From the wavelet spectrum, we estimate the following spectral indices: $\beta = 0.96 \pm 0.18$ for periods from about 4 hours up to 4 days, and $\beta = 1.87 \pm 0.03$ for periods between 1 minute and approximately 4 hours. An accurate assessment of these spectral indices is important for determining the underlying physical models.

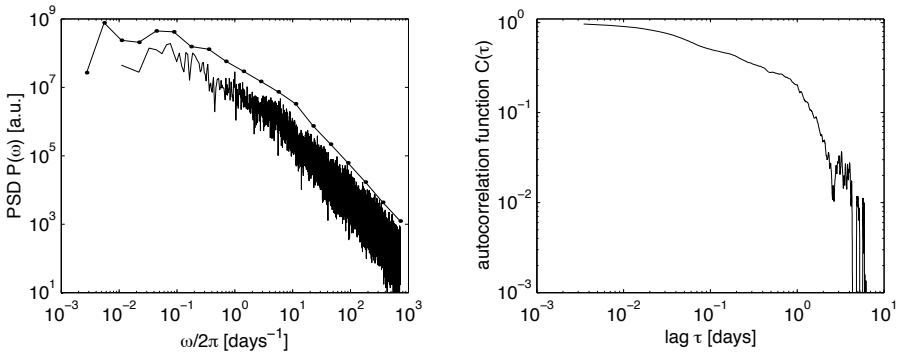

Fig. 14. Power spectrum (left) and autocorrelation function (right) of one year of AE data from 1986. The sampling period is 1 minute. The power spectrum was estimated using a periodogram with 5 windows, and the wavelet spectrum (dots) with 4th order Daubechies wavelets. The wavelet scales are connected to frequencies by $\omega = 1/a$. The two spectra have been shifted vertically to ease comparison.

Autocorrelation Many simple physical models (i.e. Markov models, autoregressive models) give rise to exponentially decaying autocorrelation functions.

Such a functional dependence means that the process has a characteristic time scale (or spatial scale). For scale invariant processes, the autocorrelation function should instead decay algebraically

$$C(\tau) \propto \tau^{-\gamma} \ , \tag{31}$$

where the exponent is connected to the spectral index by $\gamma = 1 - \beta$. Strictly speaking, a process is called long-range correlated when $0 < \gamma < 1$.

Unfortunately, autocorrelation functions provide a poor estimate of the indices β and γ [7]. This is illustrated in Fig. 14: note how difficult it is to recognize a power law scaling in the autocorrelation function; an exponential gives almost as good a fit.

Waiting time statistics Another candidate for an unambiguous indication of long-range dependence and in particular SOC, is the waiting-time statistics. The idea is to consider the interval between bursts rather than the burst size. Many simple models yield distributions of intervals that follow a Poisson distribution with exponential tails, whereas scale invariant systems should give a power law. See [25] for an application to the AE index. These methods are receiving today much attention in the context of solar physics, see [2].

The problem here is merely a question of properly estimating the pdf and finding a sufficiently long range over which a power law can be meaningfully assessed. For the estimation of pdfs see [65].

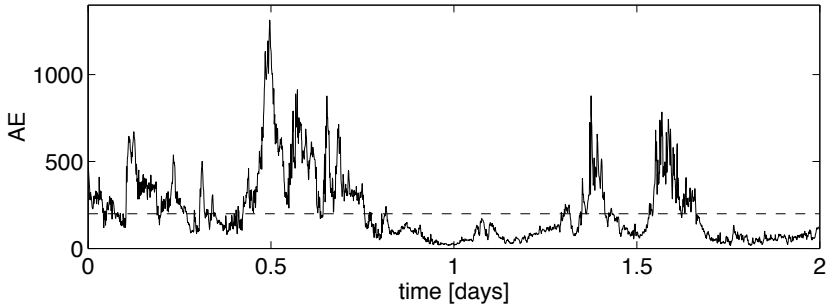

Fig. 15. Excerpt of the AE index data. Waiting times are based on the intervals between each successive crossing of the $AE = 200$ line.

An example is shown in Fig. 16, again based on one year of AE index data. An excerpt of the time series is shown in Fig. 15. We computed the duration of the intervals between successive values where the index cross the $AE = 200$ amplitude line. Changing this level does not significantly affect the results as long as it stays in the bulk of the distribution. The pdf of the time intervals clearly shows a power law scaling that extends over almost two decades (left plot), and which can definitely not be fitted with an exponential (right plot).

For small intervals, the results are indicative of the magnetospheric dynamics, whereas long intervals may be affected by external driving terms such as the solar wind, hence the deviation from the power law scaling.

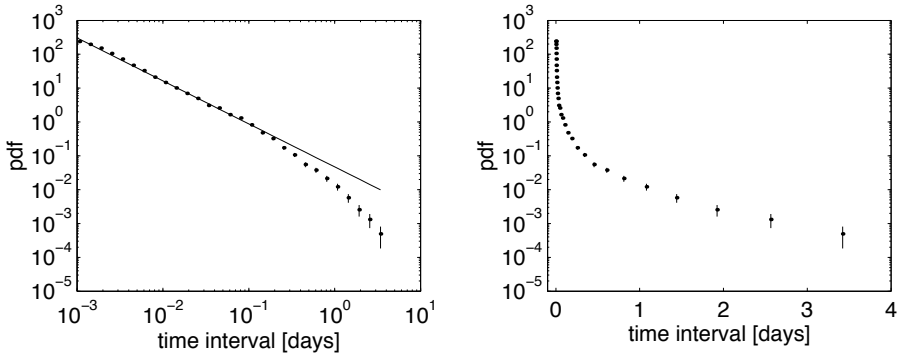

Fig. 16. Waiting time statistics for the AE index in 1986. The pdfs of the time intervals between successive crossings of the $AE = 200$ amplitude are shown. Left plot is with log-log axes and plot with lin-log axes.

Other measures One can think of many other possible measures for long-range dependence; the main problem is to keep physical insight. The *Hurst exponent* is a quantity that has been popular lately in laboratory plasma experiments, but which should be used with caution. The method itself is called *Hurst rescaled range analysis*; it was originally proposed by Hurst, who used it to detect persisting trends in time series (see for example [42]). A recent application of the Hurst exponent to tokamak plasma turbulence was used to claim the existence of long-range dependence and SOC [15]. Similar conclusions were drawn from the analysis of AE data [56]. The problem with this quantity is its ambiguous interpretation [7].

3.3 Lévy walks and anomalous transport

Recently, a great deal of attention has been paid to anomalous (i.e. non-diffusive) transport in fluids. For low frequency magnetic turbulence and a strong background magnetic field, the motion of charged particles is approximately along the magnetic field lines. When the fluctuation level increases and/or the anisotropy of the magnetic field changes, the braided topology of the magnetic field may generate new types of transport regimes that are not necessarily diffusive anymore. This again results in scale-invariance and non-Gaussian properties.

Anomalous transport can be appropriately described in the framework of Lévy distributions [10,58]. Consider the probability distribution of the distance

and the duration of a particle trajectory between two successive bounces. Anomalous transport is intimately associated with distributions that asymptotically decay as power laws. This means that the particle has a significant probability to move long distances. Furthermore, some of the moments of the distribution (such as the mean distance, the variance, etc.) may actually diverge. Studies of Lagrangian transport of tracer particles in fluid experiments [59] and in plasma turbulence simulations [55] have revealed the mechanisms by which Lévy walks occur. The resulting anomalous transport can have an noticeable impact on macroscopic plasma properties, and may explain percolation from the solar wind into the magnetosheath.

Fig. 17. Trajectory in 2D space of a particle with Brownian motion (left) and Lévy random walk (right).

Figure 17 compares the trajectories in 2D space of a particle with standard random walk motion (i.e. Brownian motion) and a particle that makes Lévy random walks. The first has a diffusive motion whereas the second will give super-diffusion. The characterization of such transport regimes is appropriately done by using a Lagrangian approach with test particles. Let $\langle \Delta x^2 \rangle_\tau$ be the mean square distance traveled by a particle during a time interval τ. Then

$$\langle \Delta x^2 \rangle_\tau = 2D\tau^\alpha \ ,$$

where D is the diffusion coefficient and μ the diffusion exponent. Brownian motion with standard diffusion corresponds to the case $\mu = 1$, $\mu < 1$ is called subdiffusion, $\mu > 1$ superdiffusion, and $\mu = 2$ corresponds to ballistic motion[8].

As an example we consider test particle simulations based on a 2-D model [38]. The scaling of the mean squared displacement with the observation time is shown in Fig. 18. A power law is indeed apparent over several decades. Below the ion gyrofrequency, the scaling exponent is $\alpha = 2$, in agreement with the ballistic nature of the ion gyration. Above the gyrofrequency, however, the exponent α stays close to 1.8, thereby suggesting that the motion is neither diffusive, nor ballistic. The deviation at largest time intervals is a finite sample size effect.

[8] Note that for processes with Gaussian statistics, the value of μ is connected to the spectral index β.

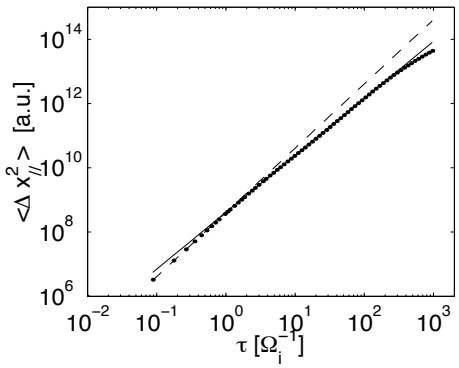

Fig. 18. Scaling of the mean square displacement along the magnetic field vs travel time τ. The slopes of the straight lines are $\mu = 1.8$ (full line) and $\mu = 2.0$ (dashed line).

4 Outlook

The development of techniques for characterizing nonlinear processes is a challenging and rapidly expanding area. However, as the techniques tend to become more and more sophisticated, there appears the risk of losing physical insight. It is indeed tempting to gather many techniques in a toolbox, and then start doing data mining.

In the next decades, significant outbreaks are expected (or at least hoped for) in the following areas:

- The analysis of spatio-temporal processes, which include data from multi-point measurements, 1D, 2D and 3D models. Our capacity of analyzing data dramatically drops as soon as a spatial dimension comes in, and most of the results obtained so far are still based on time-domain techniques.
- As we increasingly have to deal with large and multivariate data sets with a lot of redundant information, there is also a growing need for doing pre-processing. This involves "reducing" the number of significant variables to make them more tractable. It also means locating interesting features in the data. Many techniques have been developed for that purpose, using either classical methods (e.g. principal component analysis) or more novel concepts such as artificial intelligence.
- Models have a significant advantage over experiments: they can produce long records of data with a very low noise level. Many nonlinear models in addition show signatures of low-dimensional determinism, and therefore lend themselves for a characterization of chaotic behaviour. Tools that have been developed for that purpose (e.g. [57]) can nowadays provide deep insight into the analytical properties of such models.

References

1. H. D. I. Abarbanel, R. Brown, and J. J. Sidorovich: *The analysis of observed chaotic data in physical systems*, Rev. Mod. Phys. 65, 1331-1392 (1993).
2. M. J. Aschwanden, B. R. Dennis, and A. Benz: *Logistic Avalanche Processes, Elementary Time Structures, and Frequency Distributions in Solar Flares*, Astrophysical Journal 497, 972-993 (1998).
3. P. Abry, P. Gonçalvès, and P. Flandrin: *Wavelets, spectrum estimation,* $1/f$ *processes*, in *Wavelets and Statistics*, edited by A. Antoniadis and G. Oppenheim, Lecture Notes in Statistics, Vol. 103 (Springer, Berlin, 1995), pp. 15-30.
4. E. Bacry, J.F. Muzy, and A. Arneodo: *Singularity spectrum of fractal signals from wavelet analysis: exact results*, J. Stat. Phys. 70, 635-674 (1993).
5. R. Badii and A. Politi: *Complexity* (Cambridge Univ. Press, Cambridge, 1997).
6. S. D. Bale, D. Burgess, P. J. Kellogg, K. Goetz, R. L. Howard, and S. J. Monson:*Evidence of three-wave interactions in the upstream solar wind*, Geoph. Res. Lett., 23, 109-112 (1996).
7. J. Beran: *Statistics for long-memory processes*, (Chapman & Hall, London, 1994).
8. D. Biskamp: *Nonlinear magnetohydrodynamics*, (Cambridge Univ. Press, Cambridge, 1993).
9. T. Bohr, M. H. Jensen, G. Paladin, and A. Vulpiani: *Dynamical systems approach to turbulence*, (Cambridge Univ. Press, Cambridge, 1998).
10. J.-P. Bouchaud and A. Georges: *Anomalous diffusion in disordered media: statistical mechanisms, models, and physical applications*, Phys. Reports 195, 127-293 (1990).
11. D. R. Brillinger: *Time series*, (Holt, New York, 1975).
12. L. F. Burlaga: *Multifractal structure of the interplanetary magnetic field*, Geoph. Res. Lett. 18, 69-72 (1991).
13. V. Carbone: *Scaling exponents of the velocity structure functions in the interplanetary medium*, Ann. Geoph, 12, 585-590 (1994).
14. V. Carbone, P. Giuliani, L. Sorriso-Valvo, P. Veltri, R. Bruno, E. Martines, and V. Antoni: *Intermittency in plasma turbulence*, Planet. Space Sci., in the press.
15. B. A. Carreras, B. P. van Milligen, M. A. Pedrosa, et al.: *Experimental evidence of long-range correlation and self-similarity in plasma fluctuations*, Phys. Plasmas 6, 1885-1892 (1999).
16. A. Chhabra and R. V. Jensen: *Direct determination of the* $f(\alpha)$ *singularity spectrum*, Phys. Rev. Lett. 62, 1327-1330 (1989).
17. D. Coca, M. A. Balikhin, S. A. Billings, H. St. C. K. Alleyne, M. W. Dunlop, and H. Lühr: *Time-domain identification of nonlinear processes in space-plasma turbulence using multi-point measurements*, in *Proc. Cluster II workshop on Multiscale/Multipoint Plasma Measurements,* document ESA SP-449, ESA, Paris (2000).
18. G. Consolini, M. F. Marcucci, and M. Candidi: *Multifractal structure of the auroral electrojet index data*, Phys. Rev. Lett., 76, 4082-4085 (1996).
19. G. Consolini and T. Chang: *Magnetic field topology and criticality in GEOTAIL dynamics: relevance to substorm phenomena*, Space Science Rev. 95, 309-321 (2001).
20. T. Dudok de Wit and V. V. Krasnosel'skikh: *Wavelet bicoherence analysis of strong plasma turbulence at the Earth's quasiparallel bow shock*, Phys. Plasmas 2, 4307-4311 (1995).
21. T. Dudok de Wit and V. V. Krasnosel'skikh: *Non-Gaussian statistics in space plasma turbulence: fractal properties and pitfalls*, Nonl. Proc. Geoph. 3, 262-273 (1996).

22. T. Dudok de Wit: *Data analysis techniques for resolving nonlinear processes in plasmas: a review*, in *The URSI Review on Radio Science 1993–1995*, edited by R. E. Stone (Oxford University Press, Oxford, 1996).
23. T. Dudok de Wit, V. Krasnosel'skikh, M. Dunlop, and H. Lühr: *Identifying nonlinear wave interactions using two-point measurements: a case study of SLAMS*, J. Geophys. Res. 104, 17079-17090 (1999).
24. P. Escoubet, A. Roux, F. Lefeuvre, and D. LeQuéau (eds.): *START: Spatio-temporal analysis for resolving plasma turbulence*, document WPP-047 (ESA, Paris, 1993).
25. M. P. Freeman, N. W. Watkins, and D. J. Riley: *Evidence for a solar wind origin of the power law burst lifetime distribution of the AE indices*, Geoph. Res. Lett. 27, 1087-1090 (2000).
26. U. Frisch: *Turbulence* (Cambrisge Univ. Press, Cambridge, 1995).
27. K.-H. Glassmeier, U. Motschmann, and R. Schmidt: *CLUSTER workshops on data analysis tools, physical measurements and mission-oriented theory*, document SP-371 (ESA, Paris, 1995).
28. M. L. Goldstein and D. A. Roberts: *Magnetoshydrodynamic turbulence in the solar wind*, Phys. Plasmas 6, 4154-4160 (1999).
29. P. Grassberger and I. Procaccia: *Characterization of strange attractors*, Phys. Rev. Lett. 50, 1265 (1983).
30. M. J. Hinich and C. S. Clay: *The application of the discrete Fourier transform in the estimation of power spectra, coherence and bispectra of geophysical data*, Rev. Geoph. 6, 347-363 (1968).
31. T. S. Horbury and A. Balogh: *Structure function measurements of the intermittent MHD turbulent cascade*, Nonl. Proc. Geoph. 4, 185-199 (1997).
32. W. Horton and A. Hasegawa: *Quasi-two-dimensional dynamics of plasmas and fluids*, Chaos 4, 227-251 (1994).
33. H. J. Jensen: *Self-organized criticality* (Cambridge University Press, Cambridge, 1998).
34. B. B. Kadomtsev: *Plasma turbulence* (Academic Press, New York, 1965).
35. H. Kantz and T. Schreiber: *Nonlinear time series analysis* (Cambridge University Press, Cambridge, 1997).
36. Y. C. Kim and E. J. Powers: *Digital bispectral analysis and its applications to nonlinear wave interactions*, IEEE Trans. Plasma Sci. PS-7, 120-131 (1979).
37. V. Kravtchenko-Berejnoi, F. Lefeuvre, V. V. Krasnosel'skikh, and D. Lagoutte: *On the use of tricoherent analysis to detect non-linear wave interactions*, Signal Processing 42, 291-309 (1995).
38. Y. Kuramitsu and T. Hada: *Acceleration of charged particles by large amplitude MHD waves: effect of wave spatial correlation*, Geophys. Res. Lett. 27, 629-632 (2000).
39. J.-L. Lacoume, P.-O. Amblard, and P. Comon: *Statistiques d'ordre supérieur pour le traitement du signal* (Masson, Paris, 1997).
40. D. Lagoutte, D., F. Lefeuvre, and J. Hanasz: *Application of bicoherence analysis in study of wave interactions in space plasmas*, J. Geoph. Res. 94, 435-442 (1989).
41. L. Ljung: *System identification: theory for the user* (Prentice-Hall, Englewood Cliffs, NJ, 1999).
42. B. Mandelbrot: *Fractals and scaling in finance* (Springer Verlag, Berlin, 1997).
43. E. Marsch and C.-Y. Tu: *Non-Gaussian probability distributions of solar wind fluctuations*, Ann. Geoph. 12, 1127-1138 (1994).
44. E. Marsch: *Analysis of MHD turbulence: spectra of ideal invariants, structure functions and intermittency scalings*, in [27] pp. 107-118.

45. J. M. Mendel: *Tutorial on Higher Order Statistics (Spectra) in signal processing and system theory: theoretical results and some applications*, Proc. IEEE 79(3), 278-305 (1991).
46. S. L. Musher, A. M. Rubenchik, and V. E. Zakharov: *Weak Langmuir turbulence*, Phys. Rep. 252, 177-274 (1995).
47. J.-F. Muzy, E. Bacry, and A. Arneodo: *Multifractal formalism for fractal signals: the structure-function approach versus the wavelet-transform modulus-maxima method*, Phys. Rev. E 47, 875-884 (1993).
48. S. W. Nam and E. J. Powers: *Applications of higher order spectral analysis to cubically nonlinear system identification*, IEEE Trans. Acoust. Speech Signal Proc. ASSP-42, 1746-1765 (1994).
49. C. L. Nikias and A. P. Petropulu: *Higher-order spectra analysis* (Prentice Hall, New Jersey, 1993).
50. C. L. Nikias and M. E. Raghuveer: *Bispectrum estimation: a digital signal processing framework*, Proc. IEEE 75, 869-891 (1987).
51. G. Paladin and A. Vulpiani: *Anomalous scaling laws in multifractal objects*, Phys. Reports 4, 147-225 (1987).
52. R. K. Pearson: *Discrete-time dynamic models* (Oxford Univ. Press, Oxford, 1999).
53. H. L. Pécseli and J. Trulsen: *On the interpretation of experimental methods for investigating nonlinear wave phenomena*, Plasma Phys. Controlled Fusion 25, 1701-1715 (1993).
54. D. B. Percival and A. T. Walden: *Spectral Analysis for Physical Applications: Multitaper and Conventional Univariate Tehcniques* (Cambridge University Press, Cambridge, 1993).
55. P. Pommois, G. Zimbardo, and P. Veltri: *Magnetic field line transport in three dimensional turbulence: Lévy random walk and spectrum models*, Phys. Plasmas 5, 1288-1297 (1998).
56. C. P. Price and D. E. Newman: *Using the R/S statistic to analyze AE data*, J. Atmos. Solar-Terrestr. Phys. 63, 1387-1397 (2001).
57. T. Schreiber: *Interdisciplinary application of nonlinear time series analysis*, report WUB-98-13 (University of Wuppertal, Wuppertal, Germany, 1998) [available at http://xxx.lanl.gov/abs/chao-dyn/9807001].
58. M. F. Shlesinger, G. M. Zaslavsky, and J. Klafter: *Strange kinetics*, Nature 363, 31-37 (1993).
59. T. H. Solomon, E. R. Weeks, and H. Swinney: *Chaotic advection in a two-dimensional flow: Lévy flights and anomalous diffusion*, Physica D 76, 70-84 (1994).
60. K. Stasiewicz, B. Holback, V. Krasnosel'skikh, M. Boehm, R. Boström, and P. M. Kintner: *Parametric instabilities of Langmuir waves observed by Freja*, J. Geoph. Res. 101, 21515-21525 (1996).
61. L. Rezeau, G. Belmont, B. Guéret, and B. Lembège: *Cross-bispectral analysis of the electromagnetic field in a beam-plasma interaction*, J. Geophys. Res. 102, 24387-24392 (1997).
62. C. P. Ritz and E. J. Powers: *Estimation of nonlinear transfer functions for fully developed turbulence*, Physica D 20, 320-334 (1986).
63. C. P. Ritz, E. J. Powers, T. L. Rhodes, et al.: *Advanced plasma fluctuation analysis techniques and their impact on fusion research*, Rev. Sci. Instrum. 59, 1739-1744 (1988).
64. C. P. Ritz, E. J. Powers, and R. D. Bengtson: *Experimental measurement of three-wave coupling and energy cascading*, Phys. Fluids B 1, 153-163 (1989).
65. B. W. Silverman: *Density Estimation for statistics and data analysis* (Chapman & Hall, London, 1986).

66. D. Sornette: *Critical phenomena in natural sciences: chaos, fractals, self-organisation and disorder* (Springer Verlag, Berlin 2000).
67. J. Takalo, R. Lohikoski, and J. Timonen: *Structure function as a tool in AE and Dst time series analysis*, Geophys. Res. Lett. 22, 635-638 (1995).
68. B. P. van Milligen, E. Sánchez, T. Estrada, C. Hidalgo, B. Brañas, B. Carreras, and L. García: *Wavelet bicoherence: a new turbulence analysis tool*, ‘ Phys. Plasmas 2, 3017-3032 (1995).
69. D. V. Vassiliadis, D. N. Baker, H. Lundstedt, and R. C. Davidson (eds.): *Nonlinear methods in space plasma physics*, Phys. Plasmas 6(11), 4137-4199 (1999).
70. D. Vassiliadis: *System identification, modeling, and prediction for space weather environments*, IEEE Trans. Plasma Science, in the press.
71. N. Watkins, M. P. Freeman, S. C. Chapman, and R. O. Dendy: *Testing the SOC hpothesis for the magnetosphere*, J. Atmos. Terr. Phys., in the press.
72. V. E. Zakharov, S. L. Musher, and A. M. Rubenchik: *Hamiltonian approach to the description of non-linear plasma phenomena*, Phys. Rep. 129, 285-366 (1985).